CRITERIA FOR EVALUATING THE ACCURACY OF SURFACE TENSION VALUES FROM DIGITAL VISION SYSTEMS

Y. Z. Zhou[a]; J. Gaydos[a]

[a] Department of Mechanical & Aerospace Engineering, Carleton University, Ottawa, Canada

PLEASE SCROLL DOWN FOR ARTICLE

Taylor & Francis
Taylor & Francis Group

CRITERIA FOR EVALUATING THE ACCURACY OF SURFACE TENSION VALUES FROM DIGITAL VISION SYSTEMS

Y. Z. Zhou
J. Gaydos
Department of Mechanical & Aerospace Engineering,
Carleton University, Ottawa, Canada

Experimental techniques for measuring surface tension using the shape of either axisymmetric sessile or pendant drops have existed for many years. Recent developments in digital image acquisition and processing have permitted the computerization of the process, by which the coordinates of the drop's edge profile are obtained. Algorithms like the axisymmetric drop shape analysis−profile (ADSA−P) program use the edge profile coordinates to estimate quantities such as the surface tension, drop volume, and contact angle. The precision of these estimated quantities depends on various effects that influence the accuracy by which the edge profile coordinates are acquired. We have modeled this uncertainty in coordinate information as a perturbation effect and related the size of the perturbation to the surface tension accuracy. Two analogous relations were used to set regions of surface tension accuracy, e.g., $\pm 0.01\,mJ/m^2$ or $0.01\,mJ/m^2$ as functions of the magnification of the drop, CCD camera array size, pixel size, drop shape, and drop edge precision. An algorithm for the design of various vision systems based on these criteria will be discussed and illustrated.

INTRODUCTION

There are numerous methodologies for the measurement of contact angles and surface tensions. One of the most common methods for obtaining the interfacial tension and contact angle is based on the shape of a sessile or pendant drop. For example, the axisymmetric drop shape analysis−Profile (ADSA−P) algorithm and program of Rotenberg *et al.* [1, 2] use the edge profile coordinates of the drop to estimate quantities such as surface tension, drop volume, and contact angle. The precision of these estimated quantities depends on the accuracy of the drop's edge profile coordinates as acquired by the ADSA-P program. One method for acquiring the edge profile coordinates involves digital image acquisition, whereby the drop's image is acquired by a charge coupled device (CCD) camera and the light intensity distribution recorded on the CCD is used to determine the drop's edge profile and corresponding spatial coordinates. Any uncertainty in the vision system will affect the accuracy of the drop's profile coordinates and the precision of the surface tension [3]. Thus, to quantify the uncertainty of the digital vision system and to obtain a precision for the surface tension we will (1) estimate the experimental surface tension precision for an arbitrary vision system and (2) detail the methodology for the design of a vision system.

The ADSA−P methodology has been used in this article because software source code is available in the public domain [4] and because the ADSA−P program has been used by a number of researchers over a period of time and its reliability is well established. Extensive research developing ADSA−P as an effective tool [5−7] and using it in studies of protein adsorption [8], the wetting behaviour of poly(alkyl methacrylate) polymers [9], dynamic contact angles [10], and line tension [11−15] have occurred under the direction of or in collaboration with A. W. Neumann. Interesting and novel applications of ADSA−P have also occurred elsewhere, including a droplet evaporation study [16], an investigation of adsorbed protein layers by low-rate, dynamic liquid-fluid contact angles [17] and by analyzing bubble shapes at a water−air interface [18, 19], and the influence of binding hexadecyltrimethylammonium bromide to starch polysaccharides [20]. An evaluation of miscibility conditions for the Terra Nova oil pool, which is the second-largest oil pool discovered under the Grand Banks of the Canadian east coast, has used ADSA−P as a tool to determine interfacial tension data and to establish oil recovery selection criteria [21]. As a final example of the scope of ADSA applications, we mention the interesting study of spreading rate measurements for the

characterization of clinical treatments of grinding, acid etching, and deproteinization on medical dentin tissue [22].

The numerical integration of the Laplace equation of capillary to determine the shape of either a pendant or sessile drop is possible when values of the surface tension or capillary constant and the radius of curvature of the drop at the origin are provided [23]. In all cases, the origin is taken as the location where the drop's principal radii are equal and $R_1 = R_2 = R_0$. This integration permits one to create a theoretical/numerical drop edge profile or set of profile coordinates without any experimental errors. As shown below, the magnitude of typical numerical errors are orders of magnitude below the magnitude of typical experimental errors (*e.g.*, for pure water at 20°C experimental errors for surface tension range from a low of $\pm 0.08\,\mathrm{mJ/m^2}$ to $\pm 0.5\,\mathrm{mJ/m^2}$). If this numerical profile is perturbed (as described below) and the set of perturbed profile coordinates are used as input to the ADSA−P program (or any similarly designed software package that uses drop edge or profile points), then it is possible to estimate the relation between size of profile perturbation (detailed in several ways below) and the surface tension deviation, $\Delta \gamma$, that results from the perturbation. For area array CCD cameras with 10^6 pixels or more, the magnitude of the perturbation can be characterized in terms of pixels, so that there is a direct connection between the CCD pixel array size and the smallest possible surface tension uncertainty, $\Delta \gamma$.

In this article, by combining the numerical solution of the Laplace equation of capillary and the ADSA−P method, we were able to develop (1) a perturbation model to simulate the uncertainty in the profile coordinates and then to relate the size of the perturbation to the best surface tension precision possible and (2) two analogous relations that set regions of surface tension accuracy, *e.g.*, $\pm 0.01\,\mathrm{mJ/m^2}$ or $\pm 0.1\,\mathrm{mJ/m^2}$ as functions of the magnification of the drop, CCD camera array size, pixel size, drop shape, and drop edge precision. Finally, an algorithm for the design of a vision system based on this criterion will be discussed.

THE LAPLACE EQUATION OF CAPILLARITY FOR AXISYMMETRIC DROPS

The shape of a drop is a balance between surface tension and gravity, and this balance is reflected by the Laplace equation of capillary, given by

$$\gamma\left(\frac{1}{R_1} + \frac{1}{R_2}\right) = \gamma\left(\frac{d\theta}{ds} + \frac{\sin\theta}{x}\right) = \frac{2\gamma}{R_0} \pm \Delta\rho g z, \tag{1}$$

when the interface is symmetric about the vertical z axis and the principal radii of curvature, R_1 and R_2, are related to the arc-length, s, and the angle of inclination of the interface to the horizontal through the turning angle, θ [23]. Thus, for given values of γ and $\Delta P_0 = 2\gamma R_0$, the shape of a drop can be determined. The inverse—determination of the interfacial tension, γ from the shape—is also possible [1, 2]. This equation can be expressed in dimensionless form using the capillary constant c, defined by $c = \Delta\rho g/\gamma$, to write Equation (1) as

$$\frac{d\theta}{dS} = \frac{2}{B_0} + Z - \frac{\sin\theta}{X}, \qquad (2)$$

where the dimensionless lengths are defined as

$$S = sc^{\frac{1}{2}}; \ X = xc^{\frac{1}{2}}; \ Z = zc^{\frac{1}{2}}; \ B_0 = R_0 c^{\frac{1}{2}}. \qquad (3)$$

A procedure to perform this numerical integration using the dimensionless arc length, S, was established by Hartland and Hartley [23] and will be used to establish an ideal or perfect axisymmetric drop shape prior to any perturbation.

In the ADSA−P algorithm an objective function, defined as a measure of the absolute normal distance between the n input coordinates u_n (either experimental or numerical) and the corresponding axisymmetric Laplacian curve, v, determined uniquely by the parameters R_0 and c, is minimized as the criterion for determining a suitable fit between the input profile data points and the Laplacian curve (i.e., the curve represents an acceptable solution to Laplace's equation of capillarity for axisymmetric drops) [1, 2].

MODELLING THE DISTRIBUTION OF DROP EDGE PERTURBATION LENGTHS

A model algorithm was developed to perturb an ideal drop profile (obtained as a numerical solution to the axisymmetric Laplace equation of capillarity) and to determine the distribution of normal distances between the two profiles (ideal and perturbed). In a physical sense, a perturbation of the edge profile may come from any uncertainty within the experiment and was used as a means to simulate these experimental uncertainties so that their influence on other parameters such as the surface tension could be quantified. This knowledge may help in the design of an experimental system or with the estimation of the precision by which various parameters can be determined by the experimental system.

The Laplace equation of capillarity in the form given by Equation (2) permits one to determine the theoretical edge profile of an axisymmetric sessile or pendant drop. An extended precision program based on the algorithm of Hartland and Hartley [23] was developed to obtain a numerical solution to Laplace's equation of capillarity. This program will be referred to herein as the *Laplace program* and is available from the authors. This *Laplace program* was used to create an accurate initial drop profile (as illustrated in Figure 1 for a sessile drop). The initial profile served as a reference profile (denoted herein as Profile_0) for comparison with the perturbed profile. Profile_0 was a function of the density difference across the interface, $\Delta\rho$, surface tension, γ, and the radius of curvature of the apex of the drop, R_0. This apex point occurs at the top of a sessile drop or the bottom of a pendant drop. Alternatively, one can define a capillary constant, c, whereupon Profile_0 becomes a function of c, γ, and the dimensionless apex radius,
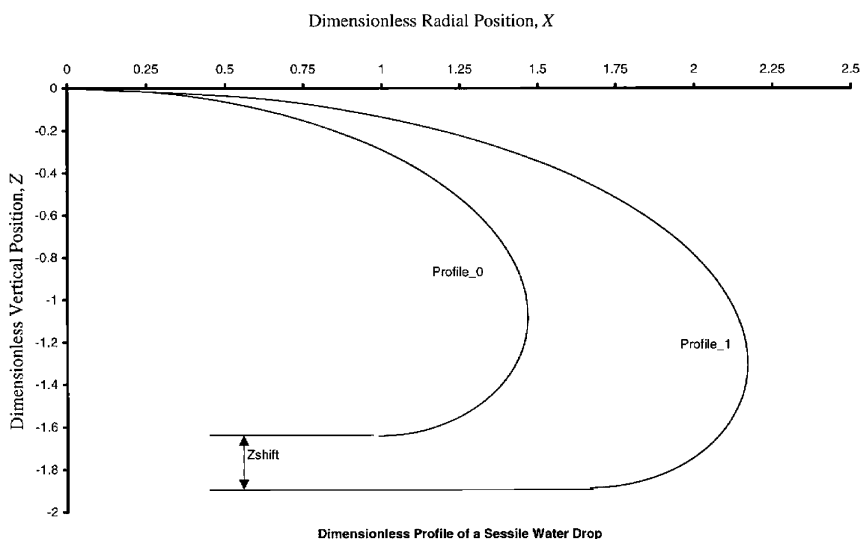
FIGURE 1 Axisymmetric sessile drop profile coordinates in dimensionless vertical and horizontal units as generated by the Laplace program using a surface tension of $72\,\text{mJ/m}^2$. The Laplace program commences the integration of the solution from the origin (top of the sessile drop) and it stops when the turning angle (or contact angle) reaches 180°. Any surface tension input or final contact angle is possible. An initial profile (Profile_0) and a perturbed profile (Profile_1) are shown with their distinct termination points. In order to compare the two drop profiles, Profile_1 must be shifted upwards by a distance, Z_{shift}, so that the two drops have identical termination elevation (or Z coordinates).

$B_0 = R_0\sqrt{c}$. A weakly perturbed profile was obtained using the Laplace program to alter B_0 and γ according to the expressions

$$\widetilde{B}_0 = B_0 + \delta B_0, \; provided \; \left|\frac{\delta B_0}{B_0}\right| << 1, \tag{4}$$

$$\widetilde{\gamma} = \gamma + \delta\gamma, \; provided \; \left|\frac{\delta\gamma}{\gamma}\right| << 1. \tag{5}$$

This perturbed profile, referred to as Profile_1, is illustrated in Figure 1. As a result of the numerical integration procedure, the initial and the perturbed profiles (*i.e.*, Profile_0 and Profile_1) do not have the same termination point or final end point. Consequently, to permit a comparison between the two profiles it was necessary to shift Profile_1 by a small vertical displacement to ensure that the end points of both profiles occur at the same horizontal elevation (distance Z*shift* in Figure 1 is accentuated for illustrative purposes). In a physical sense, this shift ensures that one compares two drops supported by the same horizontal substrate (sessile drop situation) or suspended by the same vertical tube (pendant drop situation). We denote Profile_1 after the suitable vertical shift as Profile_2 (see Figure 2). Once again, various dimensions in Figure 2 have been accentuated in scale. Comparison of Profile_0 with Profile_2 yields the distribution of normal perturbation lengths, λ, as a function of B_0, γ, and the arc-length, s, or the turning angle, θ; that is, the function $\lambda = f(B_0, \gamma, \theta, \text{ or } s)$ as shown in either Figure 2 or Figure 3. If we denote $\lambda_{\max}$ as the absolute maximum physical perturbation length for the whole arc length of the drop, then the dimensionless perturbation-length ratio, $\hat{\lambda}$, can be defined as the ratio

$$\hat{\lambda} = \frac{\lambda}{\lambda_{\max}}, \tag{6}$$

where $0 \leq \hat{\lambda} \leq 1$ and $\lambda_{\max} = \max\{\lambda; \; for \; 0 < s \leq s_{\max} \text{ or } 0 < \theta_l \leq \pi\}$. An analogous ratio can be defined for the dimensionless arc length, $\hat{s}$, as

$$\hat{s} = \frac{s}{s_{\max}}, \tag{7}$$

where $s_{\max}$ represents the maximum arc length value for the numerical integration. Thus, for integration points at positions s_i, one defines $s_{\max} = \max\{s_i, \text{ for all } i\}$. Subsequently, one may generate the function $\hat{\lambda} = f(B_0, \gamma, \theta, \text{ or } \hat{s})$ or $\hat{\lambda} = f(B_0, \gamma/\Delta\rho g R_0^2, \theta, \text{ or } \hat{s})$ for the dimensionless perturbation length ratio. This distribution, $\hat{\lambda}$, provides one with a new way to predict the displacement of the edge profile of a drop based on the original edge profile while maintaining a physically realistic
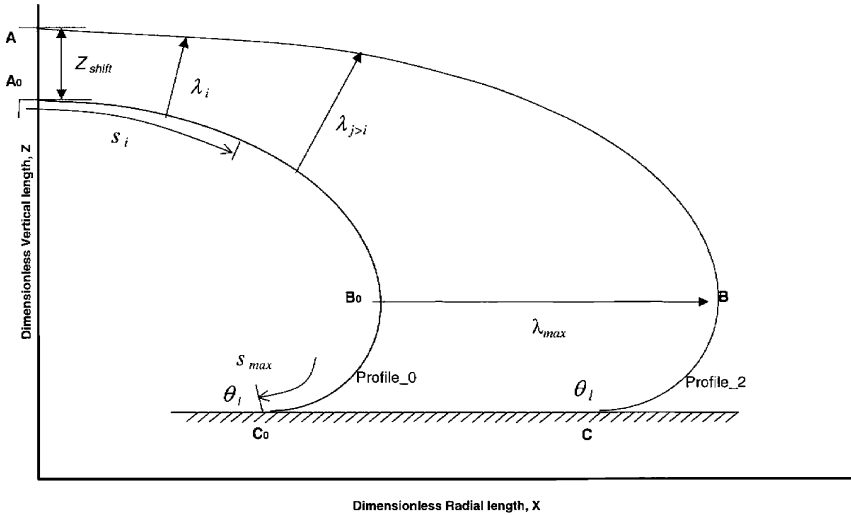
FIGURE 2 Figure 1 sessile drop profile coordinates in dimensionless vertical and horizontal units as generated by the Laplace program using a surface tension of $72\,\mathrm{mJ/m}^2$ after the Z_{shift} vertical upward shift of Profile_1. The apex points (denoted by A_0 and A) of the two drops have the same radial coordinate, and the termination points or contact points (denoted by C_0 and C) have the same vertical coordinate. The maximum physical distance between the two profiles occurs at the equator point B_0 to B.

result (*i.e.*, perturbed shape is a solution to Equation (1)). Thus, if a set of edge profile coordinates (X_i^0, Z_i^0) is given, then it is possible to create a new set of perturbed edge profile coordinates $(\widetilde{X}_i,\ \widetilde{Z}_i)$ *via* simple relations,

$$\widetilde{X}_i = X_i^0 + \delta X_i \ with \ \delta X_i = \lambda_i \cos\theta, \tag{8}$$

$$\widetilde{Z}_i = Z_i^0 + \delta Z_i \ with \ \delta Z_i + \lambda_i \sin\theta, \tag{9}$$

where $\lambda_i = \hat{\lambda}_i \lambda_{\max}$, and $\hat{\lambda}_i$ is obtained from a calculation that produces data such as that shown in Figure 3. Boundary conditions apply such that $\delta X = 0$ at the apex point (to keep the profile axisymmetric) and $\delta Z = 0$ at the contact point (to keep the sessile drop in contact with the substrate). It is important to note that these new profile coordinates, $(\widetilde{X}_i, \widetilde{Z}_i)$, will still satisfy the Laplace equation of capillary and are, therefore, physically realistic solutions for a drop. The original edge profile (X_i^0, Z_i^0) may be obtained from either a numerical integration of the Laplace equation of capillary or obtained from the image
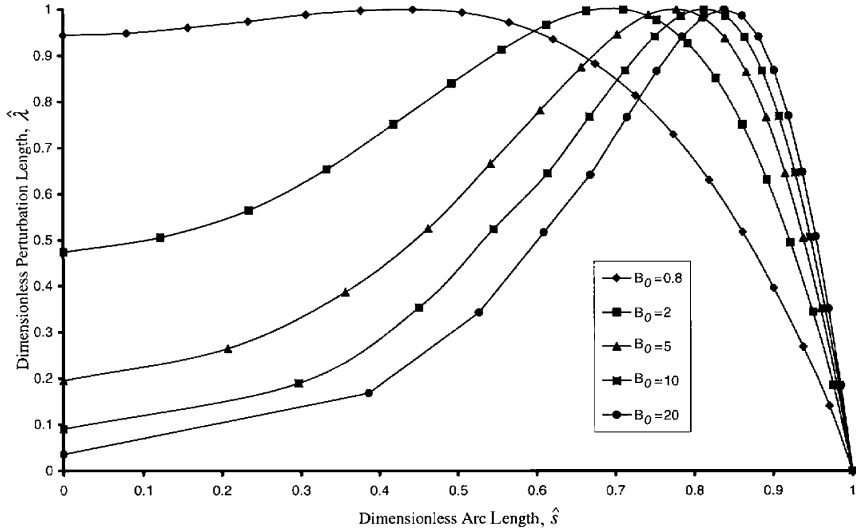
FIGURE 3 The dimensionless perturbation length ratio, $\hat{\lambda}$, as a function of the dimensionless arc length, $\hat{s}$ for various nonspherical sessile drops. The reference or unperturbed drop was taken as a drop with a surface tension $\gamma = 72\,\text{mJ/m}^2$ and a dimensionless apex curvature of $B_0 = 2$. Curves for dimensionless apex curvatures of 0.8, 2, 5, 10, and 20 are provided.

representation of the drop's edge. This perturbation modelling provides us with an accurate means of moving from an arbitrary but known edge profile to an adjacent profile that is either a slight expansion or contraction. Figures 3 through 8 illustrate various $\hat{\lambda}$ distributions that will be discussed below. In the next section we evaluate the accuracy or precision of the perturbation modelling technique.

EVALUATION OF THE PERTURBATION MODELLING APPROACH

An unperturbed set of profile coordinates can be created by the Laplace program and used as input to the ADSA−P program. ADSA−P uses these coordinates to estimate quantities such as the surface tension. When the original set of coordinates are used as input to ADSA−P, one should—and one does—recover the same value of surface tension as used as input to the Laplace program. Thus, if we perturb the original profile coordinates and use this perturbed set of coordinates as input to ADSA−P, then we will be able to estimate

the effect of profile coordinate uncertainty on the estimated surface tension value. We use this procedure to establish a connection between edge detection uncertainty and surface tension accuracy. It is important to recognize that our methodology is completely general and can be applied to any software package (not just ADSA−P). First, we evaluate the consistency of the Laplace program and the ADSA−P program using the algorithm diagrammed below. Quantities of significance in the algorithm are:

$B_0|_{Laplace}^0$: *input value to Laplace program*

$\gamma|_{Laplace}^0$: *input value to Laplace program*

$P^0\left(X_i^0, Z_i^0\right)$: *profile output from Laplace program based on input values of* $B_0|_{Laplace}^0$ *and* $\gamma|_{Laplace}^0$

$B_0|_{ADSA}^0$: *output from the ADSA−P program based on input profile* $P^0\left(X_i^0, Z_i^0\right)$

$\gamma|_{ADSA}^0$: *output from the ADSA−P program based on input profile* $P^0\left(X_i^0, Z_i^0\right)$
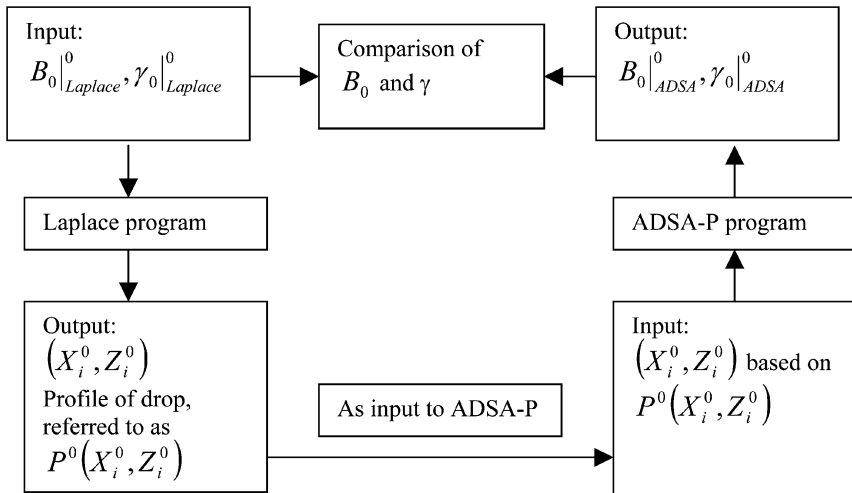
In theory the following equalities should be satisfied:

$$B_0|_{ADSA}^0 = B_0|_{Laplace}^0, \tag{10}$$

$$\gamma|_{ADSA}^0 = \gamma|_{Laplace}^0. \tag{11}$$

Table 1 illustrates this comparison.[1] Values of B_0 and γ were used as input to the Laplace program to create a set of edge profile coordinates (X_i^0, Z_i^0). These coordinates were then used as input to the ADSA−P program to determine B_0 and γ values. We used 36 points (the number of points is arbitrary but should be even if the total number is small to insure the profile is axisymmetric) plus one point at the drop's apex in all profiles [2]. As shown in Table 1, ADSA−P correctly determines B_0 and γ values to five digits from the numerically accurate profile coordinates. Several Fortran compilers on different OS platforms were used to establish this accuracy. The compilers included: Absoft Fortran v.5.1 from Absoft Inc., G77 Fortran from the Free Software Foundation (GNU) on a WinNT 4.0 OS, and F77 on SUN UNIX. The accuracy could be slightly improved if the number of points in the profile input were increased beyond 37. Typically, experimental values of surface tension have either 2 or 3 digits of accuracy, so a surface tension value of $72.1 \, \mathrm{mJ/m^2}$ is not significantly different from a value of $72.0 \, \mathrm{mJ/m^2}$. Table 1 indicates that the numerical integration of the Laplace program of capillarity (our Laplace program) was able to produce a sufficiently accurate set of profile coordinates (X_i^0, Z_i^0), and that the

TABLE 1 Comparison of ADSA−P Program Estimates of B_0 and γ Using 37 Numerically Generated Profile Coordinates from an Integration of the Laplace Equation of Capillary (Using the Laplace Program)

Case	Parameters	Laplace program	ADSA program
1	B_0	0.4	0.400103
	γ	72	72.016975
2	B_0	0.8	0.800010
	γ	72	72.008894
3	B_0	2	2.000102
	γ	72	72.004280
4	B_0	10	10.000207
	γ	72	72.000683
5	B_0	20	20.001356
	γ	72	71.997939

Surface tension, γ, in units $\mathrm{mJ/m^2}$ with B_0 dimensionless.

[1]All example data are based on a pure water sessile drop: $\Delta\rho = 1000 \, \mathrm{kg/m^3}$, $g = \mathrm{m/s^2}, \gamma = 72 \, \mathrm{mJ/m^2}$.

ADSA−P program was able to obtain consistent values of B_0 and γ from these profile coordinates. If B_0 and γ are altered by small increments δB_0 and $\delta\gamma$, so that the new values become $\widetilde{B}_0 = B_0 + \delta B_0$ and $\tilde{\gamma} = \gamma + \delta\gamma$, then these new values can be used as inputs to the Laplace program to obtain a new set of coordinates, $(X_i, Z_i)|_{new}$. If this set of coordinates is used as input to ADSA−P, then ADSA−P will produce consistent values of $\widetilde{B}_0$ and $\tilde{\gamma}$ to the suggested numerical accuracy of Table 1. The left hand side of the flow chart below illustrates the evaluation procedure and the block location where the perturbation distribution (discussed below) is obtained as a comparison between the two coordinate profiles (*i.e.,* original and perturbed profile using input $\widetilde{B}_0$ and $\tilde{\gamma}$). Alternatively, if the original set of profile coordinates is adjusted using the perturbation distribution $\lambda_i = \hat{\lambda}_i \lambda_{\max}$ instead, then the adjusted coordinates can be inserted into ADSA−P and adjusted values of $\widetilde{B}_0|_{Perturbed}^{ADSA}$ and $\tilde{\gamma}|_{Perturbed}^{ADSA}$ can be obtained for comparison. Quantities of significance in flow chart are:

$B_0|_{Laplace}^0, \gamma|_{Laplace}^0$: Original values input to the Laplace program to generate original profile with profile coordinates (X_i^0, Z_i^0).

$P^0(X_i^0, Z_i^0)$: Original set of coordinate profile points based on input values $B_0|_{Laplace}^0$, $\gamma|_{Laplace}^0$.

$\widetilde{B}_0|_{Laplace}, \tilde{\gamma}|_{Laplace}$: Perturbed values input to the Laplace program.

$\widetilde{P}|_{Laplace}(\widetilde{X}_i|_{Laplace}, \widetilde{Z}_i|_{Laplace})$: New set of profile coordinate points output from the Laplace program based on perturbed values $\widetilde{B}_0|_{Laplace}$ and $\tilde{\gamma}|_{Laplace}$.

$\widetilde{B}_0|_{Unperturbed}^{ADSA}, \tilde{\gamma}|_{Unperturbed}^{ADSA}$: Values output from ADSA−P based on input profile coordinates $\widetilde{P}|_{Laplace}(\widetilde{X}_i|_{Laplace}, \widetilde{Z}_i|_{Laplace})$ where the "unperturbed" subscript indicates that coordinates were obtained without invoking a small perturbation on the original set of coordinate points.

$\widetilde{P}|_{ADSA}(\widetilde{X}_i|_{ADSA}, \widetilde{Z}_i|_{ADSA})$: New set of perturbed profile coordinates obtained by perturbing the original drop profile, $P^0(X_i^0, Z_i^0)$, using the perturbation length distribution $\hat{\lambda} = f(B_0, \gamma, \theta \text{ or } \hat{s})$.

$\widetilde{B}_0|_{Perturbed}^{ADSA}, \tilde{\gamma}|_{Perturbed}^{ADSA}$: Values output from ADSA−P based on input drop profile $\widetilde{P}|_{ADSA}(\widetilde{X}_i|_{ADSA}, \widetilde{Z}_i|_{ADSA})$.

Input $\widetilde{P}\big|_{laplace}\left(\widetilde{X}_i\big|_{Laplace}, \widetilde{Z}_i\big|_{Laplace}\right)$ to ADSA-P program

Output is:
$\widetilde{B}_0\big|_{Un-perturbed}^{ADSA}$ and $\widetilde{\gamma}\big|_{Un-perturbed}^{ADSA}$

Input to Laplace program:
$\widetilde{B}_0\big|_{Laplace} = B_0\big|_{Laplace}^0 + \delta B_0$
$\widetilde{\gamma}\big|_{Laplace} = \gamma\big|_{Laplace}^0 + \delta\gamma$

Compare
$\widetilde{B}_0\big|_{Un-perturbed}^{ADSA}$ and $\widetilde{\gamma}\big|_{Un-perturbed}^{ADSA}$
with
$\widetilde{B}_0\big|_{Perturbed}^{ADSA}$ and $\widetilde{\gamma}\big|_{Perturbed}^{ADSA}$

Output:
$\widetilde{B}_0\big|_{Perturbed}^{ADSA}$
$\widetilde{\gamma}\big|_{Perturbed}^{ADSA}$

Laplace program

ADSA-P program

Output set of coordinates
$\left(\widetilde{X}_i\big|_{Laplace}, \widetilde{Z}_i\big|_{Laplace}\right)$
as profile of drop; denoted by
$\widetilde{P}\big|_{Laplace}\left(\widetilde{X}_i\big|_{Laplace}, \widetilde{Z}_i\big|_{Laplace}\right)$

Using $P^0\left(X_i^0, Z_i^0\right)$ with perturbation distribution
$f(\lambda_i)\left(X_i^0\big|_{Laplace}, Z_i^0\big|_{Laplace}\right)$
to obtain:
$\widetilde{X}_i\big|_{ADSA} = X_i^0 + \delta X$
$\widetilde{Z}_i\big|_{ADSA} = Z_i^0 + \delta Z$
where
$\delta X_i = \lambda_i \cos\theta$
$\delta Z_i = \lambda_i \sin\theta$
with λ_i obtained from $f(\lambda_i)$
to define coordinate profile as
$\widetilde{P}\big|_{ADSA}\left(\widetilde{X}_i\big|_{ADSA}, \widetilde{Z}_i\big|_{ADSA}\right)$

Compare
$P^0\left(X_i^0, Z_i^0\right)$
with
$\widetilde{P}\big|_{laplace}\left(\widetilde{X}_i\big|_{Laplace}, \widetilde{Z}_i\big|_{Laplace}\right)$
to obtain perturbation distribution
$f(\lambda_i)\left(X_i^0\big|_{Laplace}, Z_i^0\big|_{Laplace}\right)$

Perturbed profile used as input to ADSA-P

As we now know, based on any original profile, $\widetilde{P}\big|_{Laplace}(\widetilde{X}_i\big|_{Laplace}, \widetilde{Z}_i\big|_{Laplace})$ ADSA–P will be able to obtain values of $\tilde{B}_0\big|_{Unperturbed}^{ADSA}$ and $\tilde{\gamma}\big|_{Unperturbed}^{ADSA}$ that are numerically similar to the values of $\tilde{B}_0\big|_{Laplace}$ and $\tilde{\gamma}\big|_{Laplace}$ used as input to the Laplace program

(a numerical integration scheme for the Laplace equation of capillarity). Next, we perturb an original coordinate profile, denoted as $P^0(X_i^0, Z_i^0)$ and numerically generated using values $B_0|_{Laplace}$ and $\gamma|_{Laplace}$, to obtain a perturbed profile, denoted as $\widetilde{P}|_{ADSA}(\widetilde{X}_i|_{ADSA}, \widetilde{Z}_i|_{ADSA})$, using the perturbation length distribution, $\hat{\lambda}$. After these perturbed profile coordinates were used as input to ADSA−P, we obtained from ADSA−P estimated values of $\widetilde{B}_0|_{Perturbed}^{ADSA}$ and $\tilde{\gamma}|_{Perturbed}^{ADSA}$. If our perturbation length distribution procedure was correct, then ADSA−P should estimate values of $\widetilde{B}_0|_{Perturbed}^{ADSA}$ and $\tilde{\gamma}|_{Perturbed}^{ADSA}$, based on the input edge profile coordinates $\widetilde{P}|_{ADSA}(\widetilde{X}_i|_{ADSA}, \widetilde{Z}_i|_{ADSA})$, which are numerically equal to $\widetilde{B}_0|_{Unperturbed}^{ADSA}$ and $\tilde{\gamma}|_{Unperturbed}^{ADSA}$. The perturbation length distribution, λ, and its absolute maximum value, in particular, λ_{max}, provide the connection between the edge detection uncertainty and a robust estimation of the surface tension uncertainty. Tables 2 and 3 illustrate the level of consistency between sets $(\widetilde{B}_0|_{Laplace}, \widetilde{\gamma}|_{Laplace})$, $(\widetilde{B}_0|_{Unperturbed}^{ADSA}, \widetilde{\gamma}|_{Unperturbed}^{ADSA})$, and $(\widetilde{B}_0|_{Perturbed}^{ADSA}, \tilde{\gamma}|_{Perturbed}^{ADSA})$. Tables 2 and 3 were based on a fixed value of surface tension, $\gamma = 72$ mJ/m^2, and various values of B_0 from 0.4 to 20. All examples were based on a sessile drop configuration. An analogous comparison procedure was possible for the pendant drop configuration or for significantly different values of the surface tension.

These tabulated results in Tables 2 and 3 demonstrate that the ADSA−P program yields essentially the same (*i.e.*, results depend

TABLE 2 Perturbed Original Profile $P^0(X_i^0, Z_i^0)$, Based on Input Values of $B_0 = 0.4$ and $\gamma = 72$ mJ/m^2, to $\widetilde{P}|_{ADSA}(\widetilde{X}_i|_{ADSA}, \widetilde{Z}|_{ADSA})$

		Laplace program $\widetilde{B}_0|_{Laplace}, \tilde{\gamma}|_{Laplace}$	ADSA−P program $\widetilde{B}_0|_{Unperturbed}^{ADSA}, \tilde{\gamma}|_{Unperturbed}^{ADSA}$	ADSA−P program $\widetilde{B}_0|_{Perturbed}^{ADSA}, \tilde{\gamma}|_{Perturbed}^{ADSA}$
1	B_0	0.4001	0.4002028	0.4002034
	γ	71.9	71.9177982	71.9172713
2	B_0	0.401	0.4011028	0.4011069
	γ	71.9	71.9177520	71.9204939
3	B_0	0.402	0.4021030	0.4021108
	γ	71.8	71.8177298	71.8247887
4	B_0	0.404	0.4041034	0.4041183
	γ	71.6	71.6176628	71.6357604

Table shows that ADSA−P provides consistent values of $(\widetilde{B}_0|_{Perturbed}^{ADSA}, \widetilde{\gamma}|_{Perturbed}^{ADSA})$, $(\widetilde{B}_0|_{Unperturbed}^{ADSA}, \tilde{\gamma}|_{Unperturbed}^{ADSA})$ with $(\widetilde{B}_0|_{Laplace}, \tilde{\gamma}|_{Laplace})$.

TABLE 3 Perturbed Original Profile $P^0(X_i^0, Z_i^0)$, Based on Input Values of $B_0 = 20$ and $\gamma = 72$ mJ/m^2, to $\widetilde{P}|_{ADSA}(\widetilde{X}_i|_{ADSA}, \widetilde{Z}_i|_{ADSA})$

		Laplace program $\tilde{B}_0|_{Laplace}, \tilde{\gamma}|_{Laplace}$	ADSA–P program $\tilde{B}_0|_{Un-perturbed}^{ADSA}, \tilde{\gamma}|_{Un-perturbed}^{ADSA}$	ADSA–P program $\tilde{B}_0|_{perturbed}^{ADSA}, \tilde{\gamma}|_{perturbed}^{ADSA}$
1	B_0	20.1	20.1008565	20.0988352
	γ	71.9	71.8992135	71.9060320
2	B_0	20.2	20.2008691	20.1949812
	γ	71.8	71.7991985	71.8181138
3	B_0	20.4	20.4009431	20.3831201
	γ	71.6	71.5990512	71.6541901
4	B_0	21	21.0010250	20.9129130
	γ	71	70.9989628	71.2537498

Table shows that ADSA–P provides consistent values of $(\widetilde{B}_0|_{Perturbed}^{ADSA}, \widetilde{\gamma}|_{Perturbed}^{ADSA})$, $(\widetilde{B}_0|_{Unperturbed}^{ADSA}, \widetilde{\gamma}|_{Unperturbed}^{ADSA})$ with $(\widetilde{B}_0|_{Laplace}, \widetilde{\gamma}|_{Laplace})$.

slightly on the actual number of profile points) set of $\widetilde{B}_0$ and $\tilde{\gamma}$ values regardless of the method used to create the input edge profile coordinates. Therefore, it would seem reasonable to conclude that the method used to create a perturbation length distribution, λ, is reasonable when combined with an initial unperturbed set of profile coordinates to generate a new set of perturbed profile coordinates. It is also reasonable to view these λ perturbations as being mechanically consistent with the physically expected result that an equilibrium drop should satisfy the Laplace equation of capillarity during a perturbation. When the sessile drop is either too small (nearly spherical) or too large (nearly flat) the utility of the ADSA–P routine suffers and we must obtain the perturbation length distribution from limiting analytical solutions. These two limiting situations are discussed below.

Analytical Solutions for the Situation of Either Extremely Large or Extremely Small Sessile Drops

Two possible types of solutions exist and will be discussed below. One solution relates to extremely large, flat drops with large values of B_0 and the other solution to extremely small, nearly spherical drops with small values of B_0. Our purpose is to derive analytical solutions for the dimensionless perturbation length ratio $\hat{\lambda} = f(B_0, \gamma, \theta_l, \text{ or } \hat{s})$; see Figures 4 and 5. The analytical solutions were used to confirm (see Tables 4 and 5) that the numerical scheme was sufficiently accurate (at least four significant digits) to be used as a tool for estimating
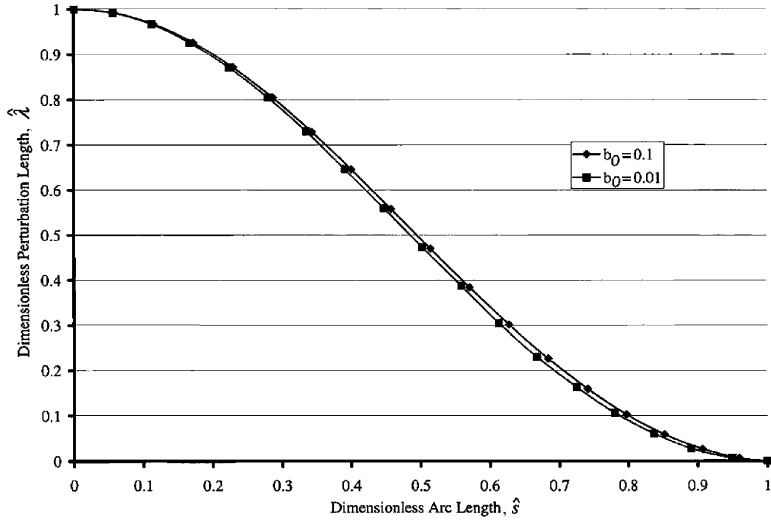
FIGURE 4 Dimensionless perturbation length ratio, $\hat{\lambda}$, as a function of the dimensionless arc length for very small, essentially spherical sessile drops. The two curves illustrate the influence of the dimensionless radius of curvature at the drop's apex (denoted by $B_0 = 0.1$ or 0.01).
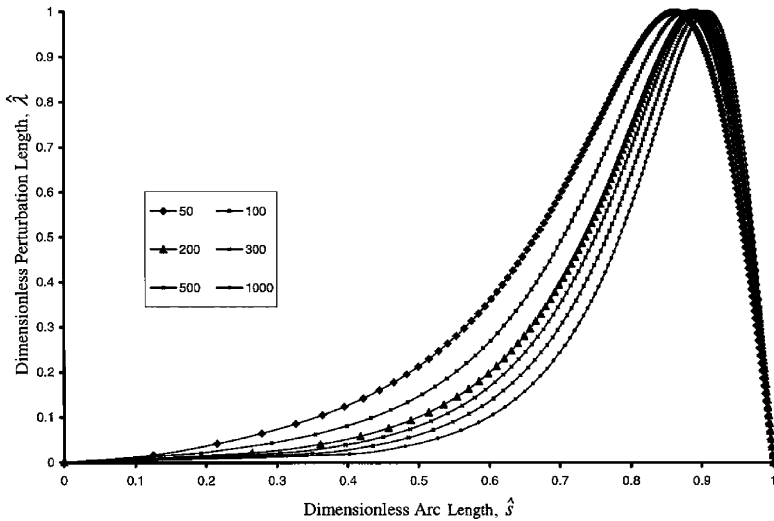
FIGURE 5 Dimensionless, normal perturbation length ratio, $\hat{\lambda}$, as a function of the dimensionless arc length, $\hat{s}$, for large, nonspherical, flat sessile drops. The curves illustrate the influence of the dimensionless radius of curvature at the drop's apex (denoted by B_0 values 50, 100, *etc.*).

TABLE 4 The Edge Profile Coordinates (X_i^0, Z_i^0) Were Determined Using the Laplace Program with $B_0 = 100$ and, the Coordinates (X_i^1, Z_i^1) Were Determined Similarly with $\widetilde{B}_0 = 105$

θ_i	X_i^0	Z_i^0	X_i^1	Z_i^1	$\delta X_i = X_i^1 - X_i^0$
10	3.868812E+00	1.830021E−01	3.922605E+00	1.834381E−01	5.379272E−02
20	4.606206E+00	3.726210E−01	4.659513E+00	3.729320E−01	5.330706E−02
30	5.009408E+00	5.577508E−01	5.062461E+00	5.579455E−01	5.305290E−02
40	5.268285E+00	7.374265E−01	5.321188E+00	7.375173E−01	5.290270E−02
50	5.442418E+00	9.104621E−01	5.495229E+00	9.104613E−01	5.281067E−02
60	5.558694E+00	1.075630E+00	5.611448E+00	1.075549E+00	5.275440E−02
70	5.631881E+00	1.231728E+00	5.684603E+00	1.231580E+00	5.272198E−02
80	5.671247E+00	1.377621E+00	5.723954E+00	1.377416E+00	5.270672E−02
90	5.683229E+00	1.512259E+00	5.735932E+00	1.512009E+00	5.270290E−02
100	5.672676E+00	1.634696E+00	5.725381E+00	1.634412E+00	5.270529E−02
110	5.643487E+00	1.744110E+00	5.696199E+00	1.743803E+00	5.271149E−02
120	5.598973E+00	1.839809E+00	5.651690E+00	1.839489E+00	5.271721E−02
130	5.542051E+00	1.921242E+00	5.594772E+00	1.920917E+00	5.272102E−02
140	5.475375E+00	1.988010E+00	5.528094E+00	1.987687E+00	5.271864E−02
150	5.401407E+00	2.039867E+00	5.454116E+00	2.039551E+00	5.270863E−02
160	5.322462E+00	2.076725E+00	5.375150E+00	2.076418E+00	5.268860E−02
170	5.240732E+00	2.098658E+00	5.293390E+00	2.098359E+00	5.265808E−02
180	5.158308E+00	2.105892E+00	5.210924E+00	2.105597E+00	5.261612E−02

The difference $\delta X_i = X_i^1 - X_i^0$ was substituted into Equation (27) to determine δZ_i. All quantities are dimensionless including the turning angle θ (in degrees) measured from the horizontal.

digital uncertainty (see Discussion of the Normal Perturbation Length Distribution, section below).

Limiting Solution for a Large Curvature Drop

If we rewrite Equation (2) as

$$\frac{1}{X}\frac{d}{dX}(X \sin \theta) = \frac{2}{B_0} \pm Z, \tag{12}$$

then the integration of Equation (12) yields

$$X \sin \theta = \frac{X^2}{B_0} \pm \int_0^X ZXdX, \tag{13}$$

Very small (large curvature) sessile and pendent drops are very nearly spherical, and the gravitation term in the pressure balance can be neglected without substantial error when B_0 is small. As a consequence, the term $2/B_0$ in Equation (12) is much greater than Z and the drop is essentially spherical (or circular with radius B_0 in a

TABLE 5 Coordinates (X_i^0, Z_i^0) Were Calculated Numerically Using the Laplace Program Based on $B_0 = 100$

θ_i	Z_i^0	δZ_i	$\tilde{Z}_i = Z_i^0 + \delta Z_i$	Z_i^1	Error (%)
10	1.830021E−01	4.511449E−04	1.834532E−01	1.834381E−01	8.219289E−03
20	3.726210E−01	3.323153E−04	3.729533E−01	3.729320E−01	5.711031E−03
30	5.577508E−01	2.264479E−04	5.579773E−01	5.579455E−01	5.695740E−03
40	7.374265E−01	1.382043E−04	7.375647E−01	7.375173E−01	6.422463E−03
50	9.104621E−01	6.739189E−05	9.105295E−01	9.104613E−01	7.487056E−03
60	1.075630E+00	1.359895E−05	1.075643E+00	1.075549E+00	8.745785E−03
70	1.231728E+00	−2.365102E−05	1.231705E+00	1.231580E+00	1.014013E−02
80	1.377621E+00	−4.508345E−05	1.377576E+00	1.377416E+00	1.160414E−02
90	1.512259E+00	−5.186920E−05	1.512207E+00	1.512009E+00	1.310262E−02
100	1.634696E+00	−4.580184E−05	1.634650E+00	1.634412E+00	1.455669E−02
110	1.744110E+00	−2.944908E−05	1.744081E+00	1.743803E+00	1.591434E−02
120	1.839809E+00	−6.243262E−06	1.839803E+00	1.839489E+00	1.707388E−02
130	1.921242E+00	1.950348E−05	1.921262E+00	1.920917E+00	1.794489E−02
140	1.988010E+00	4.270394E−05	1.988053E+00	1.987687E+00	1.840134E−02
150	2.039867E+00	5.774879E−05	2.039925E+00	2.039551E+00	1.833207E−02
160	2.076725E+00	5.892731E−05	2.076784E+00	2.076418E+00	1.762701E−02
170	2.098658E+00	4.101757E−05	2.098699E+00	2.098359E+00	1.620288E−02
180	2.105892E+00	1.641347E−11	2.105892E+00	2.105597E+00	1.402931E−02

Slightly perturbed coordinates (X_i^1, Z_i^1) were calculated numerically using the Laplace program based on $\tilde{B}_0 = 105$. Values of $\tilde{Z}_i = Z_i^0 + \delta Z_i$ were determined using Equation (58) to calculate δZ_i. A comparison of $\tilde{Z}_i$ (analytical Equation (27)) with Z_i^1 (from the Laplace program with $\tilde{B}_0 = 105$) shows that the results are not significantly different. The error was calculated using $Error = \left| \left((\tilde{Z}_i - Z_i^1) \big/ Z_i^1 \right) \times 100 \right|$ in units of percentage. All other quantities are dimensionless, including the turning angle θ (in degrees) as measured from the horizontal.

plane that includes the axis of symmetry). Thus, the equation governing the shape of this circular cross section can be written as

$$X^2 + Z^2 = 2B_0 Z. \tag{14}$$

When subjected to a small perturbation, the varied parameters alter Equation (14) to

$$(X + \delta X)^2 + (Z + \delta Z)^2 = 2(B_0 + \delta B_0)(Z + \delta Z), \tag{15}$$

so that the radial variation is given by

$$\delta X \approx \frac{Z}{X} \delta B_0 - \frac{Z - B_0}{X} \delta Z \tag{16}$$

and the vertical (along the axis of symmetry) variation by

$$\delta Z \approx \frac{Z}{Z - B_0} \delta B_0 - \frac{X}{Z - B_0} \delta X. \tag{17}$$

Thus, if we have two similar axisymmetric profiles, one denoted by $P^0(X_i^0, Z_i^0)$ and based on B_0, and another profile, denoted by $P^1(X_i^1, Z_i^1)$ and based on $\widetilde{B}_0$, such that

$$\delta B_0 = \widetilde{B}_0 - B_0 \ where \ \frac{|\delta B_0|}{|B_0|} << 1, \tag{18}$$

then the vertical distance difference between the profiles would be

$$\delta Z_i = Z_i^1 - Z_i^0. \tag{19}$$

This result, in combination with Equation (16), can be used to estimate the point-by-point radial variation, δX_i, using relation

$$\delta X_i \approx \frac{Z_i^0}{X_i^0}\delta B_0 - \frac{Z_i^0 - B_0}{X_i^0}\delta Z_i. \tag{20}$$

Analogous comments apply to the use of Equation (17) to estimate the vertical variation, δZ_i. Thus, at any point on the profile edge, the normal distance, λ_i, between two similar profiles (one profile slightly perturbed with respect to the other profile) will be given by

$$\lambda_i = \delta X_i \cos\theta + \delta Z_i \sin\theta. \tag{21}$$

Figure 4 plots the dimensionless normal perturbation length distribution, using Equation (6), for the case of small, nearly spherical drops.

Limiting Solution for very Flat Drops of Small Contact Angle and Large Curvature

Differentiating Equation (12) with respect to the dimensionless radial coordinate, X, and using the approximation that at small angles $\sin\theta$ is equivalent to $\tan\theta$ permits one to write a Bessel equation and to obtain the approximate solution [23]

$$\sin\theta \approx \frac{2}{B_0}I_1(X), \tag{22}$$

where $I_1(X)$ is a modified Bessel function of the first kind. The expression for Z, using the small angle approximation, is obtained as

$$Z = \int\limits_0^X \tan\theta \, dX \approx \int\limits_0^X \sin\theta \, dX \approx 2\int\limits_0^X \frac{1}{B_0}I_1(X)dX, \tag{23}$$

whereupon

$$Z(X) \approx \frac{2}{B_0}[I_0(X) - 1]. \tag{24}$$

The apex radius, B_0, can be eliminated from Equation (24), using Equation (22), to obtain

$$Z(X) \approx \frac{I_0(X) - 1}{I_1(X)} \sin \theta. \tag{25}$$

Equation (25) relates the dimensionless quantities, Z, X, and θ, without the use of any arbitrary constants. It is possible to obtain an analytical solution, rather than a numerical solution, for a small perturbation of a large, flat sessile drop whose profile shape is given by either Equation (24) or (25). Using Equation (24), a vertical perturbation or variation, δZ, will be connected to variations in curvature, δB_0, and radial displacement, δX, *via* the expression

$$\delta Z \approx \frac{2}{B_0} I_1(X)\delta X - 2\frac{I_0 - 1}{B_0^2}\delta B_0. \tag{26}$$

The curvature, B_0, can be replaced in Equation (26), using Equation (22), to obtain

$$\delta Z \approx \frac{I_0'I_1 - I_0 I_1' + I'}{(I_1)^2} \sin \theta \, \delta X$$
$$\approx \sin \theta \left[1 - \left(\frac{I_0}{I_1}\right)^2 + \frac{I_0}{XI_1} + \frac{I_0}{I_1^2} - \frac{1}{XI_1}\right]\delta X. \tag{27}$$

At any point on the profile edge, the normal distance between two similar profiles (one profile slightly perturbed with respect to the other profile) will be given by Equation (21), and this relation can be used in collaboration with Equation (27) to obtain an estimate of δZ when δX is varied. A comparison between this analytical approach and the numerical approach using the Laplace program demonstrates the consistency of the two approaches. This comparison is provided in Tables 4 and 5 (with $B_0 = 100$). These tables illustrate the accuracy of Equation (27) as a large drop perturbation approximation. The coordinates for the edge profile tabulated in Table 4 were created by the Laplace program and then used for comparison with the perturbed solutions. Table 5 demonstrates that the perturbation

expression, Equation (27), is acceptable when modelling the perturbation of large drop profiles.

Figure 5 shows this dimensionless perturbation length distribution for large, flat drops of small contact angle and small curvatures with B_0 values ranging from 50 to 1000 as calculated using Equation (21), with the definition in Equation (6), and Equation (27).

The analytical solution approach (applicable for either very small or large drops) permits us to obtain the normal perturbation length distribution, $\hat{\lambda} = f(B_0, \gamma, \theta, \text{ or } \hat{s})$, over a large range of B_0 values; *i.e.*, $10^{-2} \leq B_0 \leq 10^3$.

DISCUSSION OF THE NORMAL PERTURBATION LENGTH DISTRIBUTION $\hat{\lambda}$

The independent variables of the distribution, $\hat{\lambda} = f(B_0, \gamma, \theta, \text{ or } \hat{s})$, have different influences on its shape. Figure 6 illustrates the weak influence of the surface tension, γ, using a sessile drop with $\gamma = 72 \, \text{mJ/m}^2$ and $B_0 = 2$ as the reference or unperturbed configuration, on the distribution's shape. When γ is perturbed to values of 71, 60, 40, 30, and $20 \, \text{mJ/m}^2$, the corresponding $\Delta\gamma$ changes by 1, 12, 32, 42, and $52 \, \text{mJ/m}^2$, as expected, but the distribution, $\hat{\lambda}$, is not changed significantly. In contrast, Figure 7 (using the same reference configuration as in Figure 5) illustrates the strong influence of B_0. When B_0 is perturbed to 2.01, 3, 10, and 20 from its reference situation at $B_0 = 2$, the distribution $\hat{\lambda}$ has a very different shape in each case. Figure 8 illustrates the near-symmetric effect on $\hat{\lambda}$ of either slightly increasing or slightly decreasing B_0. Essentially one recovers very similar distributions for expanding and contracting drop situations. One may perturb a drop shape outward (expansion) by adding the $\hat{\lambda}$ distribution to the drop's profile or inward (contraction) by subtracting the same $\hat{\lambda}$ distribution from the drop's profile. Also, the magnitude of $\hat{\lambda}$ is strongly influenced by the turning angle, θ, or the arc length position, s. When B_0 is small, *e.g.*, $0 < B_0 < 1$, a perturbation in B_0 causes the drop profile to move in a nearly radial fashion (see Figures 3 and 4). As B_0 increases, *e.g.*, $1 < B_0 < 5$, small perturbations produce complicated profile shapes that are a combination of both vertical and horizontal shifts (see Figure 3). When B_0 is still larger, *e.g.*, $B_0 > 5$, small perturbations cause very small vertical motion [against gravity] and mostly horizontal movement (see Figures 3 and 5). In conclusion, the normalized perturbation length distribution, $\hat{\lambda}$, was primarily influenced by the size and shape of the drop, as characterized by the variables B_0 and θ or $\hat{s}$, but it was not significantly influenced by the surface tension.
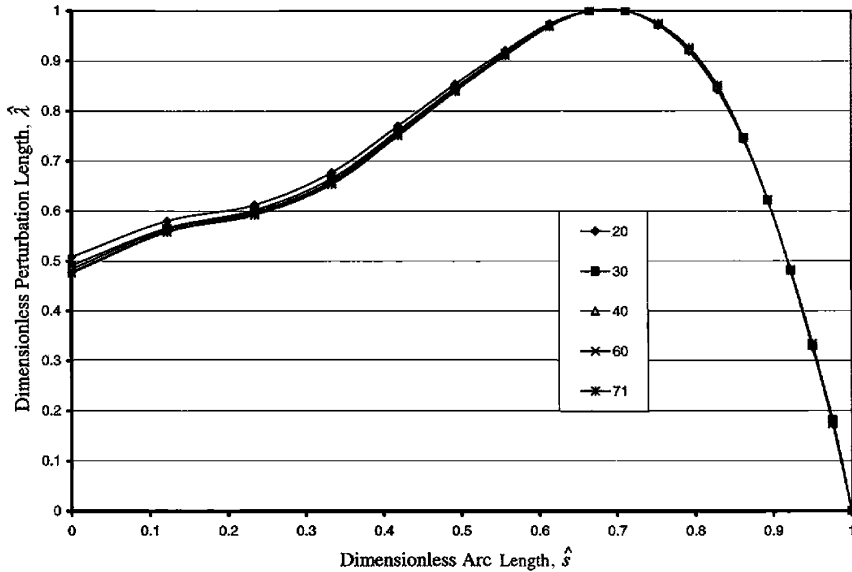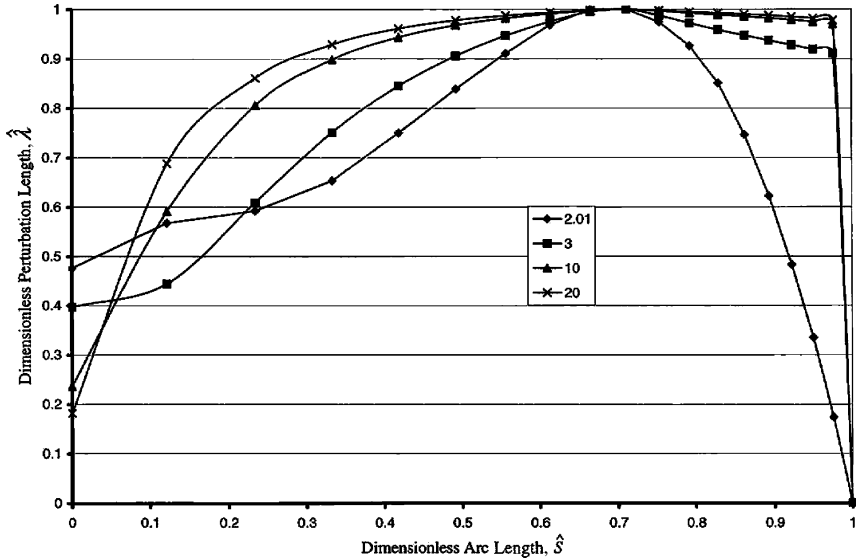
FIGURE 6 Influence of the surface tension on the dimensionless perturbation length ratio, $\hat{\lambda}$, as a function of the dimensionless arc length, $\hat{s}$, for nonspherical sessile drops. The reference or unperturbed drop was taken as a drop with a surface tension $\gamma = 72\,\mathrm{mJ/m^2}$ and a dimensionless apex curvature of $B_0 = 2$. Curves for surface tension values of 20, 30, 40, 60, and $71\,\mathrm{mJ/m^2}$ are provided.

PREDICTED SURFACE TENSION PRECISION USING THE PERTURBATION LENGTH DISTRIBUTION

The perturbation length distribution $\lambda = \lambda(B_0, \gamma, \theta, \text{ or } s)$ can be used to predict the surface tension precision ability of numerical software packages like ADSA−P. One theoretical drop profile is provided by the Laplace program (discussed above), which yields a set of very accurate drop profile coordinates (X_i^0, Z_i^0). For this original profile, we know the quantities $B_0, \gamma, \theta_{final}$, or s_{final}, where θ_{final} is the contact angle for a sessile drop. If this original profile is perturbed according to the scheme

$$\widetilde{X}_i = X_i^0 + \delta X \; with \; \left|\frac{\delta X_i}{X_i^0}\right| << 1, \tag{28}$$

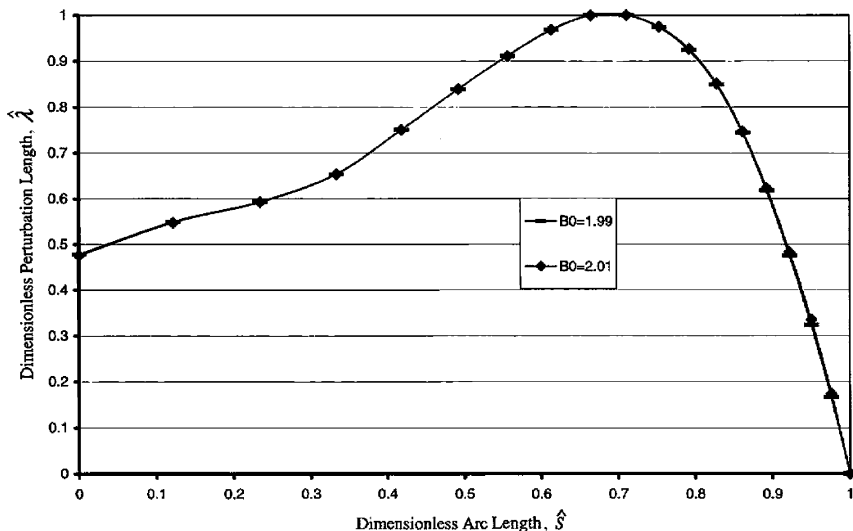$$\widetilde{Z}_i = Z_i^0 + \delta Z \; with \; \left|\frac{\delta Z_i}{Z_i^0}\right| << 1, \tag{29}$$

FIGURE 7 Influence of the dimensionless apex curvature, B_0, on the dimensionless perturbation length ratio, $\hat{\lambda}$, as a function of the dimensionless arc length, $\hat{s}$, for nonspherical sessile drops. The reference or unperturbed drop was taken as a drop with a surface tension $\gamma = 72\,\text{mJ/m}^2$ and a dimensionless apex curvature of $B_0 = 2$. Curves for dimensionless apex curvatures of 2.01, 3, 10, and 20 are provided.

then these perturbations δX_i and δZ_i can be used to obtain new coordinates for the perturbed drop profile, denoted as $(\widetilde{X}_i,\ \widetilde{Z}_i)$, and these profile coordinates can be inserted into the ADSP$-$P program to obtain a new, ADSP$-$P-based estimate of $\tilde{\gamma}$ for the perturbed drop. The surface tension change will be denoted as

$$\Delta\gamma = \tilde{\gamma} - \gamma. \tag{30}$$

Thus, if we select an original drop shape profile by selecting B_0, γ and θ_{final} or s_{final}, then we may use the appropriate perturbation length profile $\lambda = \lambda(B_0, \gamma, \theta,\ \text{or}\ s)$ to perturb the profile coordinates and obtain a corresponding perturbation, $\tilde{\gamma}$, for the drop's surface tension. A sequence of λ functions corresponding to a sequence of larger $\lambda_{\max}$ values will produce a sequence of $\tilde{\gamma}$ values and a range of $\Delta\gamma$. This relation between $\lambda_{\max}$ (the absolute maximum size of the drop's profile perturbation) and $\Delta\gamma$ (the corresponding shift in surface tension) permits one to access surface tension precision as a function of profile coordinate precision. Figure 9 plots four sets of surface tension precisions, $\Delta\gamma$; that is, surface

FIGURE 8 Influence of either slightly increasing or decreasing the dimensionless apex curvature, B_0, on the dimensionless perturbation length ratio, $\hat{\lambda}$, as a function of the dimensionless arc length, $\hat{s}$, for nonspherical sessile drops. The reference or unperturbed drop was taken as a drop with a surface tension $\gamma = 72\,\mathrm{mJ/m^2}$ and a dimensionless apex curvature of $B_0 = 2$. Curves for a dimensionless apex curvature of either 1.99 or 2.01 are shown almost on top of one another.

tension precisions at values of $\pm 1\,\mathrm{mJ/m^2}$, $\pm 0.5\,\mathrm{mJ/m^2}$, $\pm 0.1\,\mathrm{mJ/m^2}$ and $\pm 0.01\,\mathrm{mJ/m^2}$ with corresponding absolute maximum perturbation lengths, $\lambda_{\max}$, as a function of the dimensionless radius of curvature, B_0.

The surface tension change, $\Delta\gamma$, is a function of various parameters, such as B_0, γ, and the normal perturbation length distribution, $\hat{\lambda} = \hat{\lambda}(B_0, \gamma, \theta, \text{ or } \hat{s})$. The $\hat{\lambda}$ values plotted in Figure 3 include the full range of possible sessile drop configurations up to and including the unphysical contact angle $\theta_l = \pi$ (or $\hat{s}_{final} = 1$). The value of the actual or effective maximum physical perturbation length, λ_{eff}, for a particular situation depends on the shape of the drop and the location where the profile stops. As most sessile drop systems occur for situations where $\theta_l < \pi$, it is necessary to define a factor f,

$$f = \max\left\{ \hat{\lambda} = \frac{\lambda}{\lambda_{\max}}; \text{ for } 0 \leq \hat{s} \leq \hat{s}_{final} \leq 1 \right\}, \tag{31}$$

to address this limited turning angle or arc-length situation. This f factor is restricted to the range $0 \leq f \leq 1$ because $0 \leq \hat{\lambda} \leq 1$, and it changes drastically with both the location of the final arc length position, s_{final},
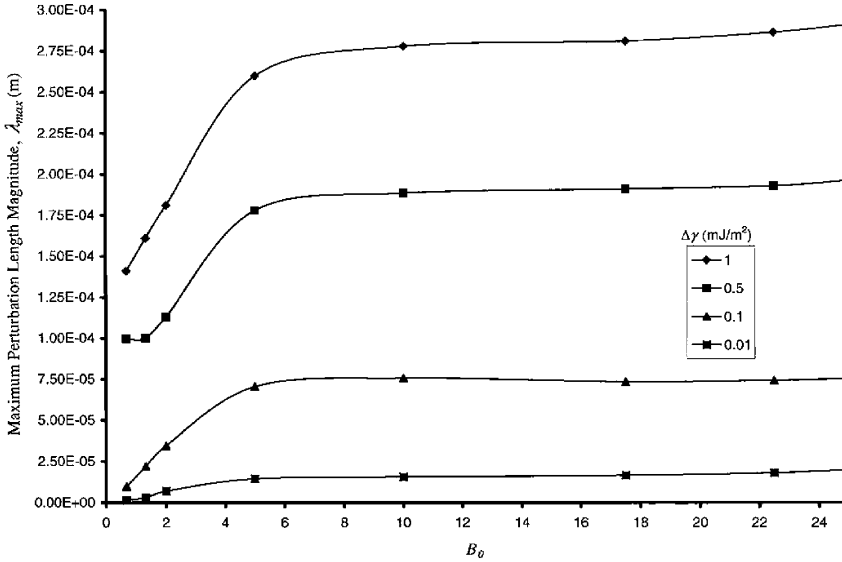
FIGURE 9 Precision of the surface tension measurement, $\Delta\gamma$, as a function of the maximum perturbation length, λ, present on a sessile drop with initial apex curvature B_0.

and the shape of drop, defined by B_0. The final arc length value, s_{final}, will correspond to a contact angle $\theta_l < \pi$, and the effective maximum perturbation length for a particular situation will equal $f\lambda_{\max}$; that is,

$$\lambda_{eff} = \max\{\lambda, \ for \ 0 \leq s \leq s_{final} \leq 1\} = f\lambda_{\max}. \tag{32}$$

If we consider a sessile drop situation with $B_0 = 2$, then we may contrast the effect of changing the contact angle θ_l on the f factor. When $\theta_l = \pi$ or $\hat{s}_{final} = 1$ (the full,theoretically possible range of values), then we know $f = 1$ and $\lambda_{eff} = \lambda_{\max}$ somewhere within the arc-length range $0 \leq \hat{s} \leq 1$. In fact, $\lambda_{eff} = \lambda_{\max}$ or $\hat{\lambda} = 1$ occurs at $\hat{s} = 0.69$ (see Figure 3). In contrast, when $\theta_l = \pi/18$, for example, the λ_{eff} value (corresponding to a value of $\hat{\lambda} = 0.12 < 1$) occurs at $\hat{s} = 0.506$, where $f = 0.12$ (see Figure 3). Consequently, for this small contact angle drop the maximum perturbation length displacement of the drop's profile will occur at the contact line, and its size will be approximately $\frac{1}{8}$ of the size that would occur for an identically shaped drop (same B_0) with a much larger contact angle. Alternatively, for a drop of a particular shape (same B_0) we may interpret these results another way. Since each $\hat{\lambda}$ curve for fixed B_0 is also a reflection of the surface tension change, $\Delta\gamma$, we may also conclude that it would be necessary to devise an experimental system that
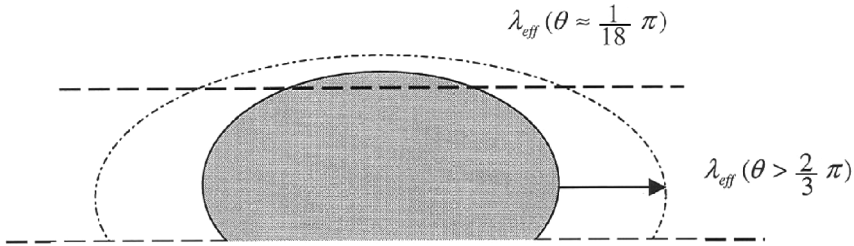
FIGURE 10 Illustration of how the effective normal perturbation, λ_{eff}, is changed with contact angle, θ_l, or final arc length, s_{final}, position on a sessile drop. For example, in this sketch (not to scale), $\lambda_{eff}(\theta_l \approx \frac{1}{18}\pi)$ is about $\frac{1}{18} \times \lambda_{eff}(\theta_l > \frac{2}{3}\pi)$ when $B_0 = 2$.

is eight times as sensitive to drop edge profile coordinate positions when using a small-angle sessile drop ($\theta_l \approx \pi/18$) instead of a large-angle sessile drop ($\theta_l > 2/3\pi$; see Figure 10). When B_0 is not fixed but the dimensionless arc-length point is fixed, say at a value $\hat{s}_{final} = 0.1$, the f factor changes. For example, when $B_0 = 5$ then $f = 0.22$, whereas when $B_0 = 0.8$ then $f = 0.96$.

These considerations would seem to imply that we may use λ_{eff} as a simple variable to show the relationship between the surface tension change or precision, $\Delta\gamma$, the maximum perturbation length, $\lambda_{\max}$, and the drop shape, B_0.

CRITERION FOR EVALUATING THE PRECISION OF THE OPTICAL SYSTEM FOR THE MEASUREMENT OF SURFACE TENSION

When we speak about an experimental system or digital vision system with specified surface tension precision, there are two questions that must be considered: (1) what is the surface tension precision level for a particular experimental system, *e.g.*, a vision system; and (2) the inverse—if we require a certain surface tension precision, how do we select various components to achieve suitable parameters and satisfy the requirement that $\Delta\gamma$ be sufficiently small?

Recently, digital image technology has become very important in the study of interfacial tensions. In this section, we develop a criterion that may be used to assess the relationship between the various parameters of a vision system, such as its magnification, pixel size and CCD sensor array, etc., and the level of the surface tension precision. Five possible situations arise in the development of a vision systems.

They are as follows:

1. Situation 1: If we know the requirement for surface tension precision, $(\Delta\gamma)_{req}$, and the drop information, such as the maximum size of the drop, $2X_{\max}$, and either the contact angle θ_l or s_{final}, then we can determine the CCD sensor parameters: P (pixel size), N (area array size), and the magnification of optical lens, M, to achieve $(\Delta\gamma)_{req}$.
2. Situation 2: If we know the camera information, P and N, the magnification of the optical lens, M, the drop information, such as $2X_{\max}$ and either θ_l or s_{final}, then we can determine the best surface tension precision, $\Delta\gamma$, that is theoretically possible.
3. Situation 3: If we know the camera information, P and N, and the requirement, $(\Delta\gamma)_{req}$, then we can select the magnification of optical lens, M, to satisfy the surface tension precision, $(\Delta\gamma)_{req}$.
4. Situation 4: If we know the camera information, P and N, and the requirement, $(\Delta\gamma)_{req}$, then we can select the approximate drop size range to use so as to satisfy this surface tension requirement.
5. Situation 5: If we know the magnification of the optical lens, M, the drop shape and the surface tension precision requirement, $(\Delta\gamma)_{req}$, then we can select the CCD camera parameters, P and N, to achieve $(\Delta\gamma)_{req}$.

An algorithm is provided for experimental situations 1 and 4 to assist readers when using the criterion to select parameters of a vision system to meet their requirements and to estimate the level of surface tension precision that is possible. Practical examples (based on a pure water sessile drop) are provided to illustrate the method and design procedure. There are six related parameters that determine surface tension:

1. The drop shape information: $2X_{\max}$, θ_l, or s_{final}. Variable $2X_{\max}$ is the maximum potential length for the drop. It is anticipated that a sessile drop will have its maximum length in the horizontal direction (perpendicular to the gravitational field vector), while a pendant drop will have its maximum length in the vertical direction (parallel to the gravitational field vector). In addition, we need an estimate for either the contact angle, θ_l, or the maximum axisymmetric arc-length distance, s_{final}, as measured from the apex origin (at the top of a sessile drop and bottom of a pendant drop).
2. The level of surface tension precision that is required, $(\Delta\gamma)_{req}$.
3. The magnification of the optical lens system, M.
4. CCD sensor parameters, P and N, where P represents the maximum physical pixel size for a CCD camera with pixel dimensions $P_1 \times P_2$, such that $P = \max(P_1, P_2)$. The variable N represents

the minimum number of pixels in either row or column of the CCD area array of dimension $N_1 \times N_2$, such that $N = \min(N_1, N_2)$.

5. Drop edge precision, $|\pm N_v|$, in units of pixels.
6. The perturbation length distribution, λ, and the f factor to characterize the extent of the distribution since $\theta_l < \pi$ (or $\hat{s} < 1$) in most cases. In the situation considered below, we set λ_{eff} to the largest effective maximum using the relation $\lambda_{eff} = f\lambda_{\max}$. SI units are meters for both $\lambda_{\max}$ and λ_{eff}.

The precision of a vision system can be described by the following criterion:

$$N_c = \frac{\lambda_{eff}M}{P}, \tag{33}$$

where the lateral or transverse magnification, M, is defined by the ratio [24]

$$M = \text{Image Size/Object Size} = \frac{PN}{2X_{\max}}, \tag{34}$$

and N_c is one criterion for establishing the precision of the surface tension (discussed below). After substituting Equation (34) into Equation (33), we obtain

$$N_c = \frac{\lambda_{eff}N}{2X_{\max}}. \tag{35}$$

Thus, if the precision of the drop's edge is given as $|\pm N_v|$, then one possible criterion for evaluating the precision of the optical system for a surface tension measurement will be

$$N_c \geq |\pm N_v|. \tag{36}$$

DISCUSSION OF CRITERION

As we know, a CCD area array camera has a photosensitive surface composed of tiny light sensitive regions called pixels. These pixels may be square ($P_1 = P_2$) or they may have an aspect ratio P_1/P_2 that is not equal to unity. Inexpensive and common CCD cameras have area arrays of 640 pixels by 480 pixels with a typical pixel size of 13 μm. Cameras with greater resolution are possible and many research level cameras have array sizes of 4 K by 4 K with individual pixels around 6.5 μm. An individual pixel is the smallest unit of resolution on a CCD array and all images recorded by the CCD camera are binned into a two dimensional array of pixels. The determination of the edge of a drop is achieved subject to this pixel array and the precision to which the pixels
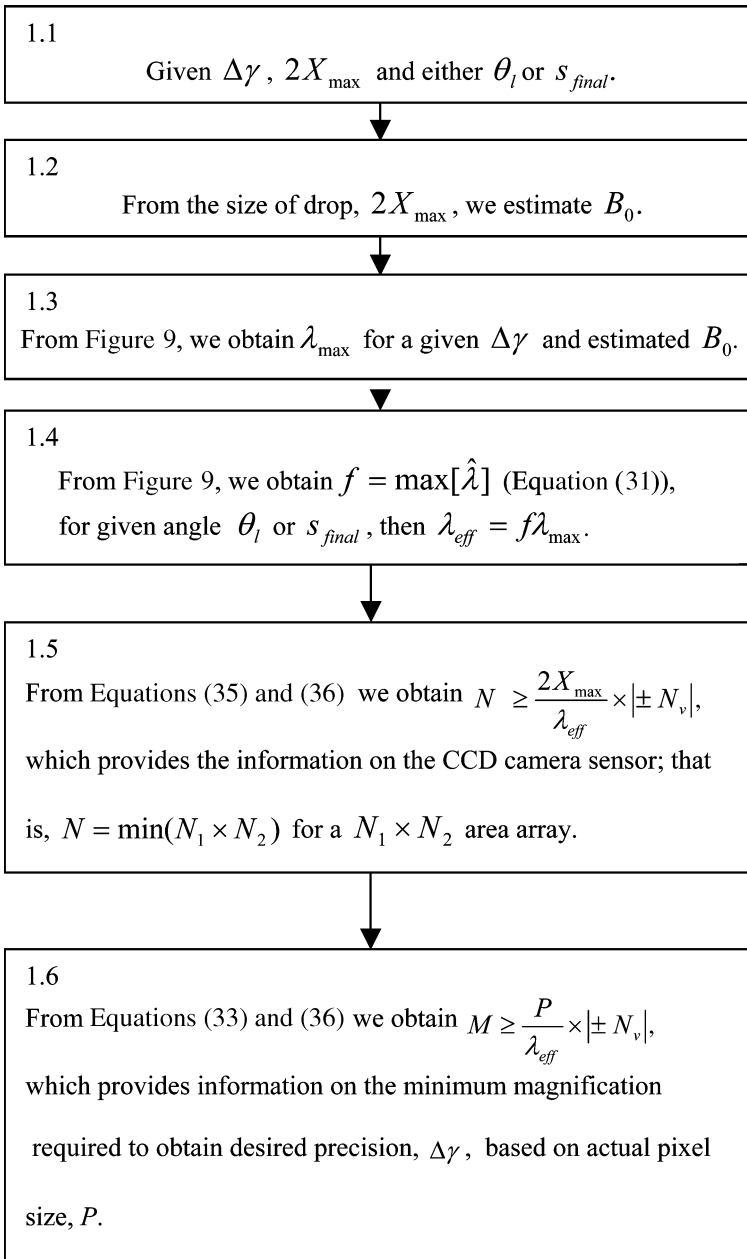
permit the edge to be positioned. In many cases, the drop's edge crosses several pixels and the edge is set as the location (or pixel) closest to the point were the light intensity gradient is a maximum. While some authors have suggested that the intensity information can be used to achieve sub-pixel resolution, we feel that it is more prudent to set the lower limit of resolution at one pixel. During image capture by the CCD camera, frame grabber, etc. every component of vision system may introduce distortions into image. In general, the edge detection precision, $|\pm N_v|$, will be influenced by many complicated effects and parameter $|\pm N_v|$ must include all the errors for every component of the vision system. Possible system error sources include: (1) software subsystem (including errors from the operating system and related software and from the edge detection algorithms used by image processing software); (2) optical subsystem (including lens distortion, blur, blooming, CCD sensor and random noise, aspect ratio, and scaling); (3) vibration control; (4) handling and position control (including leveling and vertical misalignment of the camera); (5) precision of the frame grabber subassembly; (6) characteristics of the lighting subassembly (including uniformity of the source). Thus, it will be assumed that $\min(|\pm N_v|) = 1$, where $|\pm N_v|$ is the detectable edge precision in number of pixels for the vision system. If the precision to which the edge of a drop can be estimated is 2 pixels, then we set $\min(|\pm N_v|) = 2$ pixels as the vision system position uncertainty in pixels. The criterion, N_c, for evaluating the precision of the optical system for a surface tension measurement, will then be determined by the requirement that $N_c \geq |\pm N_v|$ for all possible combinations of P, N, M, $(\Delta\gamma)_{req}$, and drop shape.

We may understand the parameter N_c in a physical sense by considering the ratio $\lambda_{eff}M/P$ of Equation (33) when M = 1 (no magnification) and the total vision system error is $\min(|\pm N_v|) = 1$ pixel. In this situation, $N_c = \lambda_{eff}/P$. Recognizing that the smallest CCD unit in the sensor array is a pixel of size P, we conclude that the optical system will not distinguish any dimension smaller than one pixel and that the criterion for detecting a perturbation of the drop's edge must be $\lambda_{eff}/P \geq 1$ or $N_c \geq 1$. If $\lambda_{eff}/P < 1$, then the vision system will not sense the perturbation or change to the drop's edge. The following section provides a few concrete situations that mimic experimental situations and the analysis algorithm for each situation.

SITUATION 1

If we know the requirement for surface tension precision, $(\delta\gamma)_{req}$, and the drop shape information, such as the maximum size of the drop $2X_{\max}$ and either θ_l or s_{final}, then we can determine the CCD sensor

parameters, P and N, and the magnification of optical lens M to achieve $(\delta\gamma)_{req}$. We proceed as follows:

1.1

Given $\Delta\gamma$, $2X_{max}$ and either θ_l or s_{final}.

1.2

From the size of drop, $2X_{max}$, we estimate B_0.

1.3

From Figure 9, we obtain λ_{max} for a given $\Delta\gamma$ and estimated B_0.

1.4

From Figure 9, we obtain $f = \max[\hat{\lambda}]$ (Equation (31)),

for given angle θ_l or s_{final}, then $\lambda_{eff} = f\lambda_{max}$.

1.5

From Equations (35) and (36) we obtain $N \geq \dfrac{2X_{max}}{\lambda_{eff}} \times \left|\pm N_v\right|$,

which provides the information on the CCD camera sensor; that

is, $N = \min(N_1 \times N_2)$ for a $N_1 \times N_2$ area array.

1.6

From Equations (33) and (36) we obtain $M \geq \dfrac{P}{\lambda_{eff}} \times \left|\pm N_v\right|$,

which provides information on the minimum magnification

required to obtain desired precision, $\Delta\gamma$, based on actual pixel

size, P.

Example 1

If we know the surface tension precision requirement $(\Delta\gamma)_{req} \approx 0.1 \, \text{mJ/m}^2$, the drop shape information $2X_{max} \approx 8 \, \text{mm}$ with $\hat{s}_{final} = 1$ (physically, this means a contact angle of $\theta_l = \pi$), and an edge precision of $|\pm N_v| = 3$, then we can determine parameters of the optical CCD camera system—that is, P, N, and M—as follows:

Step 1. Based on $2X_{max} \approx 8 \, \text{mm}$, we estimate $B_0 = 2$.

Step 2. Based on Figure 9, for given $\Delta\gamma$ and B_0, obtain $\lambda_{max} = 3.46 \times 10^{-5} \, \text{m}$.

Step 3. Based on Figure 3 with $\hat{s} = 1$ given, we obtain $f = \max[\hat{\lambda}] = 1$, so that

$$\lambda_{eff} = f\lambda_{max} = 3.46 \times 10^{-5} \, \text{m}.$$

Step 4. Using Equations (35) and (36) we obtain

$$N \geq \frac{2X_{max}}{\lambda_{eff}} \times |\pm N_v| \approx 690.$$

Step 5. Using Equation (34) and the above relation we obtain

$$M \geq \frac{P}{\lambda_{eff}} \times |\pm N_v|,$$

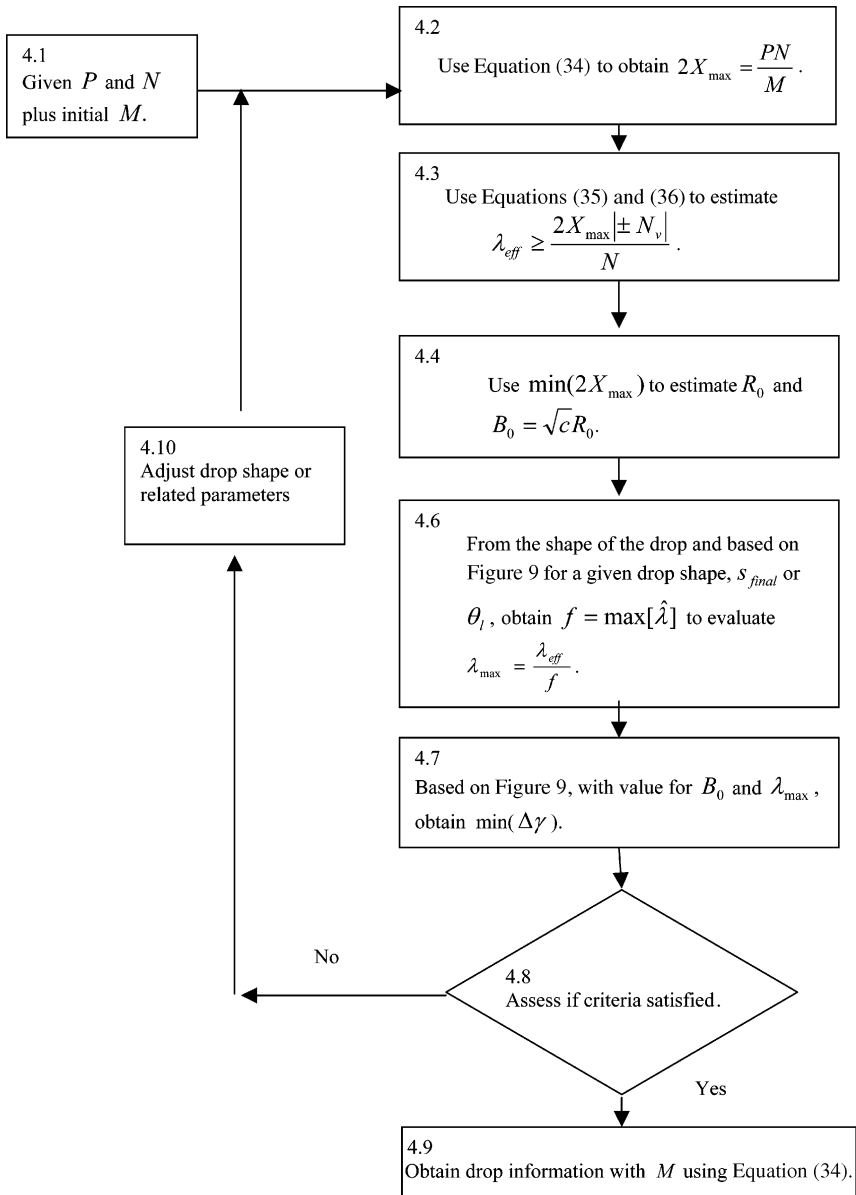and the result $M \geq 0.87$ for the most common pixel size $P \approx 10 \, \mu\text{m}$.

If $P \approx 20 \, \mu\text{m}$, then the magnification must be increased to $M \geq 1.73$.

In conclusion, a surface tension precision of $(\Delta\gamma)_{req} \approx 0.1 \, \text{mJ/m}^2$ is possible for a drop with a maximum size of $2X_{max} \approx 8 \, \text{mm}$ when the uncertainty is $|\pm N_v| = 3$ pixels, provided the magnification $M \geq 0.87$ and the CCD camera has both array dimension greater than 690 pixels and its pixel size is $P \approx 10 \, \mu\text{m}$.

SITUATION 4

If given camera information P and N, and surface tension requirement $(\delta\gamma)_{req}$, then we can select the approximate drop size necessary to satisfy the surface tension precision requirement $(\delta\gamma)_{req}$

as follows:

4.1
Given P and N plus initial M.

4.2
Use Equation (34) to obtain $2X_{max} = \dfrac{PN}{M}$.

4.3
Use Equations (35) and (36) to estimate
$$\lambda_{eff} \geq \frac{2X_{max}\left|\pm N_v\right|}{N}.$$

4.4
Use $\min(2X_{max})$ to estimate R_0 and $B_0 = \sqrt{c}\,R_0$.

4.10
Adjust drop shape or related parameters

4.6
From the shape of the drop and based on Figure 9 for a given drop shape, s_{final} or θ_l, obtain $f = \max[\hat{\lambda}]$ to evaluate
$$\lambda_{max} = \frac{\lambda_{eff}}{f}.$$

4.7
Based on Figure 9, with value for B_0 and λ_{max}, obtain $\min(\Delta\gamma)$.

4.8
Assess if criteria satisfied.

No

Yes

4.9
Obtain drop information with M using Equation (34).

Example 2

If the camera information is already known—for example, $P = 10\,\mu m$ and $N = 500$, with the requirement for surface tension precision set at $(\Delta\gamma)_{req} \approx 0.1\,mJ/m^2$, and initial drop shape information of, $2X_{max} \approx 8\,mm$, $\hat{s}_{final} = 0.14$ $(\theta_l = 10^0)$ for a sessile drop, and the precision of the vision system is estimated as $|\pm N_v| = 2$, then we may determine the parameters of the optical system, that is, M, as follows:

Step 1. Based on $2X_{max} \approx 8\,mm$, we estimate $B_0 = 2$.

Step 2. Using Equations (35) and (36), we obtain the estimate

$$\lambda_{eff} \geq \frac{2X_{max}|\pm N_v|}{N} \approx 3.2 \times 10^{-5}\,m.$$

Step 3. Based on Figure 3, given $\hat{s}_{final} = 0.14$, we obtain $f = \max[\hat{\lambda}] = 0.485$, so

$$\lambda_{max} = \frac{\lambda_{eff}}{f} = 6.6 \times 10^{-5}\,m.$$

Step 4. Based on Figure 9, for given λ_{max} and B_0, we obtain the inequality $\Delta\gamma > 0.1\,mJ/m^2 > (\Delta\gamma)_{req}$, which indicates that this CCD vision system will not be able to deliver the required surface tension precision; namely, $\Delta\gamma \leq 0.1\,mJ/m^2$. One may see why this occurs by using the criterion. From Figure 9, if we required $(\Delta\gamma)_{req} \approx 0.1\,mJ/m^2$ when $B_0 = 2$, then $\lambda_{max} \approx 3.46 \times 10^{-5}\,m$, so the effective value is $\lambda_{eff} = f\lambda_{max} = 1.68 \times 10^{-5}\,m$, which is smaller than the value estimated above and is thus not discernible. If we use Equations (35) and (36), then we can obtain an estimate of the minimum CCD array size necessary to achieve the required surface tension precision as

$$\therefore N \geq \frac{2X_{max}}{\lambda_{eff}} \times |\pm N_v| \approx 480|\pm N_v|\ then\ N \geq 960,\ when\ |\pm N_v| = 2.$$

Consequently, a digital CCD camera with an array dimension of just 500 pixels is too coarse to permit surface tension measurements at the level of precision required. One possible solution is to increase N to a value above 1000. For example, if we repeat the previous Steps 1 to 4 with $N = 1200$ we obtain

$$\lambda_{eff} \geq \frac{2X_{max}|\pm N_v|}{N} \approx 1.33 \times 10^{-5}\,m,$$

whereupon

$$\lambda_{\max} = \frac{\lambda_{eff}}{f} = 2.74 \times 10^{-5}\, \text{m}.$$

Thus, based on Figure 9, for calculated $\lambda_{\max} = 2.74 \times 10^{-5}\,\text{m} \leq 3.45 \times 10^{-5}$ and $B_0 = 2$, we obtain $\Delta\gamma < 0.1 = \text{mJ/m}^2 (\Delta\gamma)_{req}$, which satisfies the surface tension requirement. For this $N = 1200$ camera situation, the magnification M will be

$$M \approx \frac{P}{\lambda_{eff}} \times |\pm N_v| \approx 1.5.$$

Another possible solution is to change the final arc-length position of the pendant drop or the contact angle of the sessile drop. This alternative is more difficult to achieve in most practical situations but is included here to illustrate the effect of the f parameter. If given $\hat{s}_{final} = 0.56[\theta_l = 50]$ for a sessile drop, then $f = \max[\hat{\lambda}] = 0.92$ and the effective length changes to

$$\lambda_{eff} \geq \frac{2X_{\max}|\pm N_v|}{N} \approx 3.2 \times 10^{-5}\, \text{m},$$

with

$$\lambda_{\max} = \frac{\lambda_{eff}}{f} = 3.48 \times 10^{-5}\, \text{m}.$$

Using Figure 9, for $\lambda_{\max} = 3.48 \times 10^{-5}\,\text{m}$ and $B_0 = 2$, we obtain a $\Delta\gamma$ that is very close to $0.1\,\text{mJ/m}^2 = (\Delta\gamma)_{req}$ because the criterion on $\lambda_{\max}$ for $\Delta\gamma \approx 0.1\,\text{mJ/m}^2$ is $3.46 \times 10^{-5}\,\text{m}$. Thus, the minimum CCD array size, N, can be estimated as

$$N \approx \frac{2X_{\max}}{\lambda_{eff}} \times |\pm N_v| = 500,$$

and a CCD camera with a minimum array of 500 pixels will be able to achieve surface tension measurements at the precision $\Delta\gamma \leq 0.1\,\text{mJ/m}^2$ when the pixel uncertainty is $|\pm N_v| = 2$ pixels. Subsequently, the resulting best magnification can be estimated as

$$M \approx \frac{P}{\lambda_{eff}} \times |\pm N_v| \approx 0.63.$$

If we improve the vision system precision $|\pm N_v|$ to one pixel from two, then

$$N = 500,$$

$$\lambda_{eff} \geq \frac{2X_{\max}|\pm N_v|}{N} \approx 1.6 \times 10^{-5}\,\mathrm{m},$$

$$\lambda_{\max} = \lambda_{eff}/f = 3.3 \times 10^{-5}\,\mathrm{m}.$$

Thus, based on Figure 9, for given $\lambda_{\max} = 3.3 \times 10^{-5}\,\mathrm{m} \leq 3.45 \times 10^{-5}$ and $B_0 = 2$, we obtain $\Delta\gamma < 0.1\,\mathrm{mJ/m^2} = (\Delta\gamma)_{req}$, which satisfies the surface tension precision requirement.

Example 3

If the camera information is already known, for example, $P = 10\,\mathrm{\mu m}$ and $N = 1200$, with the surface tension precision requirement set at $(\Delta\gamma)_{req} \approx 0.01\,\mathrm{mJ/m^2}$, information on the drop shape given as $2X_{\max} \approx 8\,\mathrm{mm}, \hat{s}_{final} = 0.27\ (\theta_l \approx 30)$ for a sessile drop, and the precision of the vision system set at $|\pm N_v| = 2$ pixels, then we can determine the parameters of the optical system as follows:

Step 1. Based on $2X_{\max} \approx 8\,\mathrm{mm}$, we estimate $B_0 = 2$.
Step 2. Using Equations (35) and (36) we obtain

$$\lambda_{eff} \geq \frac{2X_{\max}|\pm N_v|}{N} \approx 1.33 \times 10^{-5}\,\mathrm{m}.$$

Step 3. Based on Figure 3, if given $\hat{s} = 0.27$, we obtain $f = \max[\hat{\lambda}] = 0.6$, so that

$$\lambda_{\max} = \frac{\lambda_{eff}}{f} = 2.22 \times 10^{-5}\,\mathrm{m}.$$

Step 4. Based on Figure 9, for given $\lambda_{\max}$ and B_0, we obtain the inequality $\Delta\gamma > 0.01\,\mathrm{mJ/m^2} = (\Delta\gamma)_{req}$, which indicates that this system will not satisfy the criterion because the criterion for $\lambda_{\max}$ at the surface tension precision $\Delta\gamma \approx 0.1\,\mathrm{mJ/m^2}$ is the smaller number $7.0 \times 10^{-6}\,\mathrm{m}$.

One solution is to determine the minimum CCD camera N value that would be necessary to achieve this surface tension precision. Using Figure 9 for the given $\Delta\gamma$ and B_0 of Example 2, we obtain $\lambda_{\max} = 7 \times 10^{-6}\,\mathrm{m}$ (as given above) and

$$\lambda_{eff} = f\lambda_{\max} = 4.2 \times 10^{-6}\,\mathrm{m}.$$

Finally, we use Equations (35) and (36) to estimate this array size value as

$$N \geq \frac{2X_{\max}}{\lambda_{eff}} \times |\pm N_v| = 3800,$$

which indicates that a CCD camera with $N = 1200$ is too small to satisfy the criterion on the surface tension precision when $|\pm N_v| = 2$ pixels. In the current CCD sensor market, a large CCD sensor array of this size is expensive. To achieve even higher surface tension precisions; that is, for $(\Delta\gamma)_{req} \approx 0.01\,\mathrm{mJ/m^2}$, one possible solution is to reduce $|\pm N_v|$. For example, when $|\pm N_v| = 1$, the criterion for N is reduced from $N \approx 3800$ to $N \approx 2000$, and it is possible to get a $2K \times 2K$ CCD sensor array more easily. At subpixel edge detection resolutions such as $|\pm N_v| = 0.5$, the criterion for N is further reduced to $N \approx 1000$. If we consider a $2K \times 2K$ CCD sensor array with $|\pm N_v| = 1$, then based on Equations (35) and (36) we obtain

$$\lambda_{eff} \geq \frac{2X_{\max}|\pm N_v|}{N} = 4.0 \times 10^{-6}\,\mathrm{m},$$

$$M \approx \frac{P}{\lambda_{eff}} \times |\pm N_v| \approx 2.5$$

as the required magnification that is necessary to achieve the surface tension precision. The simple conclusion is that the required surface tension precision influences the parameters of the vision system dramatically.

CONCLUSIONS

The concept of a normal perturbation length distribution, $\hat{\lambda} = \hat{\lambda}(B_0, \gamma, \theta, \text{or } \hat{s})$ was developed to relate experimental uncertainties to the surface tension precision of any software algorithm that uses the drop's edge profile to estimate the surface tension. This normal perturbation distribution is strongly influenced by the drop shape; that is, the initial B_0 value for the drop and the final arclength position, s_{final}, or tuning angle, θ. Based on this normal perturbation length distribution, several parameters were considered when evaluating the precision of surface tension values obtained for axisymmetric drop systems using a digital vision system and the ADSA−P software. The parameters were the drop shape information, $X_{\max}$, θ_l, or s_{final}, the level of surface tension precision that is required, $(\Delta\gamma)_{req}$, the magnification of the optical lens system, M, the CCD sensor parameters, P (pixel size) and N (area array size),

the drop edge precision, $|\pm N_v|$, and the perturbation length distribution, λ. Using the criterion in Equation (36) and the definitions in Equations (33) and (34), we can either estimate the surface tension precision level for a particular system or we can select various system components to achieve suitable parameters and satisfy a predefined surface tension accuracy $(\Delta\gamma)_{req}$.

REFERENCES

[1] Rotenberg, Y., Boruvka, L., and Neumann, A. W., *J. Colloid Interface Sci.* **93**, 169−183 (1983).
[2] Lahooti, S., Del Rio, O. I., Cheng, P., and Neumann, A. W., In: *Applied Surface Thermodynamics* (Marcel Dekker, New York, 1996), Chap. 10, pp. 441−507.
[3] Atae-Allah, C., Cabrerizo-Vilchez, M. A., Gomez-Lopera, J. F., Holgado-Terriza, J. A., Roman-Roldan, R., and Luque-Escamilla, P. L., *Measurement Sci. Technol.* **12**, 288−298 (2001).
[4] Rotenberg, Y., The Determination of the Shape of Non-Axisymmetric Drops and the Calculation of Surface Tension, Contact Angle, Surface Area and Volume of Axisymmetric Drops, Ph.D. Thesis, University of Toronto, Toronto, Canada (1983), Appendix F.
[5] Del Rio, O. I. and Neumann, A. W., *J. Colloid Interface Sci.* **196**, 136−147 (1997).
[6] Del Rio, O. I., Kwok, D. Y., Wu, R., Alvarez, J. M., and Neumann, A. W., *Colloids Surf. A* **143**, 197−210 (1998).
[7] Bateni, A., Susnar, S. S., Amirfazli, A., and Neumann, A. W., *Colloids Surf. A* **219**, 215−231 (2003).
[8] Susnar, S. S., Chen, P., Del Rio, O. I., and Neumann, A. W., *Colloids Surf. A* **116**, 181−194 (1996).
[9] Kwok, D. Y., Wu, R., Li, A., and Neumann, A. W., *J. Adhesion Sci. Technol.* **14**, 719−743 (2000).
[10] Lam, C. N. C., Ko, R. H. Y., Yu, L. M. Y., Ng, A., Hair, M. L., and Neumann, A. W., *J. Colloid Interface Sci.* **243**, 208−218 (2001).
[11] Gaydos, J. and Neumann, A. W., *J. Colloid Interface Sci.* **120**, 76−86 (1987).
[12] Gaydos, J. and Neumann, A. W., *Adv. Colloid Interface Sci.* **49**, 197−248 (1994).
[13] Gaydos, J. and Neumann, A. W., In: *Applied Surface Thermodynamics* (Marcel-Dekker, New York, 1996), Chap. 4, pp. 169−238.
[14] Chen, P., Gaydos, J., and Neumann, A. W., *Langmuir* **12**, 5956−5962 (1996).
[15] Amirfazli, A., Keshavarz, A., Zhang, L., and Neumann, A. W., *J. Colloid Interface Sci.* **265**, 152−160 (2003).
[16] Erbil, H. Y., McHale, G., Rowan, S. M., and Newton, M. I., *Langmuir* **15**, 7378−7385 (1999).
[17] Grundke, K., Wemer, C., Poschel, K., and Jacobasch, H. J., *Colloids Surf. A* **156**, 19−31 (1999).
[18] Makievski, A. V., Loglio, G., Kragel, J., Milles, R., Fainerman, V. B., and Neumann, A. W., *J. Phys. Chem. B* **103**, 9557−9561 (1999).
[19] Miller, R., Fainerman, V. B., Makievski, A. V., Kragel, J., Grigoriev, D. O., Krazakov, V. N., and Sinyachenko, O. V., *Adv. Colloid Interface Sci.* **86**, 39−82 (2000).
[20] Lundqvist, H., Eliasson, A. C., and Olofsson, G. *Carbohydrate Polymers* **49**, 43−55 (2002).
[21] Rao, D. N. and Lee, J. I. *J. Petroleum Sci. Eng.* **35**, 247−262 (2002).

[22] Wege, H. A., Aguilar, J. A., Rodriguez-Valverde, M. A., Toledano, M., Osorio, R. and Cabrerizo-Vilchez, M. A., *J. Colloid Interface Sci.* **263**, 162–169 (2003).

[23] Hartland, S. and Hartley, W., *Axisymmetric Fluid-Liquid Interfaces* (Elsevier Sci., Amsterdam, 1976).

[24] Hecht, E., *Optics*, 2nd ed., (Addison-Wesley, Reading, MA, 1987), p. 144.